

# Approaching Small Molecule Prioritization as a Cross-Modal Information Retrieval Task through Coordinated Representation Learning

Samuel G. Finlayson<sup>1 †</sup>, Matthew B.A. McDermott<sup>2</sup>, Alex V. Pickering<sup>3</sup>, Scott L. Lipnick<sup>3</sup>,  
William Yuan<sup>4</sup>, Isaac S. Kohane<sup>3</sup>

<sup>1</sup>*Department of Systems, Synthetic, and Quantitative Biology, Harvard Medical School, Boston, MA*

<sup>2</sup>*Department of Electrical Engineering and Computer Science, Massachusetts Institute of Technology, Cambridge, MA*

<sup>3</sup>*Department of Biomedical Informatics, Harvard Medical School, Boston, MA*

<sup>4</sup>*Department of Biological and Biomedical Sciences, Harvard Medical School, Boston, MA*

<sup>†</sup>*E-mail: samuel\_finlayson@hms.harvard.edu*

Modeling the relationship between chemical structure and molecular activity is a key task in drug development and precision medicine. In this paper, we utilize a novel deep learning architecture to jointly train coordinated embeddings of chemical structures and transcriptional signatures. We do so by training neural networks in a coordinated manner such that learned chemical representations correlate most highly with the encodings of the transcriptional patterns they induce. We then test this approach by using held-out gene expression signatures as queries into embedding space to recover their corresponding compounds. We evaluate these embeddings' utility for small molecule prioritization on this new benchmark task. Our method outperforms a series of baselines, successfully generalizing to unseen transcriptional experiments, but still struggles to generalize to entirely unseen chemical structures.

*Keywords:* Small Molecule Prioritization, Gene Expression, Deep Learning, Information Retrieval

## 1. Introduction

Identifying molecules that are likely to have a specific biological effect is a cornerstone of drug discovery and a key component of efforts to achieve precision medicine.

Classically, computational prioritization of small molecules for new indications has centered on predicting molecular affinities for specific biological targets. To this end, computational chemistry has developed a rich toolkit of methods, ranging from biophysics-driven techniques such as molecular docking<sup>1</sup> to more recent advances in machine-learning that enable allow end-to-end learning of predictive models from raw molecular graphs.<sup>2,3</sup> Additional methods leverage the literature or curated knowledge graphs to annotate molecules.<sup>4</sup> Structure-driven approaches to drug development are promising, in part, because they can be applied to novel compounds in order to prioritize testing with more expensive assays. A limitation of this paradigm when it comes to approaching new diseases, however, is that it generally assumes a priori knowledge of specific targets that one hopes to manipulate in order to achieve therapeutic effect.

More recently, connectivity mapping has emerged as a complementary approach to drug development.<sup>5</sup> In connectivity mapping, compounds are foremost characterized not by specific targets or chemical properties, but by the broad transcriptional effects they induce in

cells. Organizations such as the Broad Institute and the Library of Integrated Network-based Cellular Signatures (LINCS) Consortium have enabled the production of public datasets<sup>6,7</sup> of more than a million experiments, in which gene expression is measured in cells that have been treated with various molecular (and genetic) perturbations. Fueled by this data, researchers have sought to compute purely functional descriptions of small molecules’ effects, and use these signatures to try to match drugs in an unbiased manner to new indications and even to specific patients.<sup>8-14</sup> Connectivity mapping is promising, in part because it can be used to discover new indications of drugs while requiring very minimal assumptions about their mechanism of action. However, current approaches to connectivity mapping are generally limited to small molecules whose perturbational effects have been directly measured using gene expression assays or whose transcriptional signatures can be inferred from other experiments as by Hodos et al.<sup>15</sup>

In this paper, we attempt to merge these two paradigms by learning aligned embeddings of chemical structure and perturbational signatures (See Figure 1). We do so by training neural networks in a coordinated manner such that learned chemical representations correlate most highly with the encodings of the transcriptional patterns they induce. We then test this approach by using held out gene expression signatures as queries into the embedding space and recover their corresponding compounds.

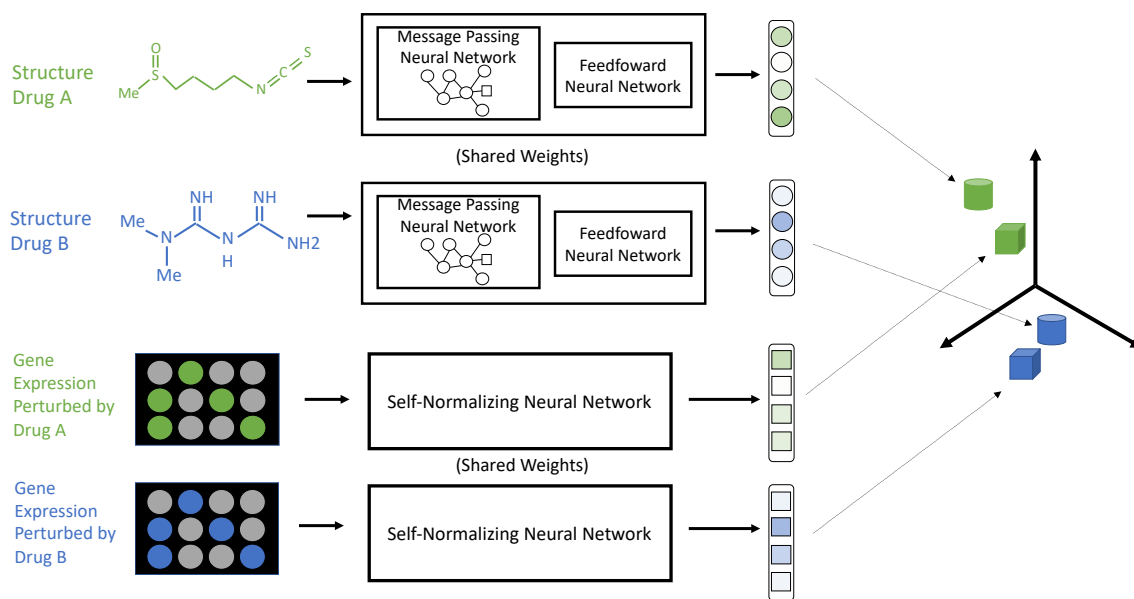


Fig. 1. Overview of our coordinated representation learning method. Neural networks are jointly trained to embed gene expression profiles and small molecule structures such that transcriptional signatures are brought into close proximity with their corresponding perturbagens. Given a cross-modal alignment, gene expression signatures can then be used as queries to rank chemical structures by their likelihood to induce such a signature.

If successful, this approach may combine some of the positive elements of structure-driven

and connectivity-driven approaches to compound prioritization: like connectivity mapping, it can be used to rank drugs from transcriptional signatures in a target-free manner. And like classic QSAR methods, once the chemical encoder is trained, it can in principle be applied to existing compound libraries in silico to nominate molecules to be run through more expensive assays. The results of our experiments demonstrate that this paradigm shows promise, but that the task of generalizing to new compounds proves particularly challenging.

## 2. Background: Multi-View Representation Alignment and Deep Embedding Learning

*Multi-view representation learning* seeks to learn representations that relate information from multiple views of the same data, such as an image of a scene and a text description of that same scene. In *multi-view representation alignment*, embeddings of each data modality are learned separately but in a coordinated manner, such that different views of the same scene are induced to be similar per some metric. In *multi-view representation fusion*, data from different views of the same scene are integrated into a single, more compact and potentially richer representation. In this work, we attempt to learn *aligned* representations of gene expression perturbational signatures and small molecules’ structures, such that gene expressions are embedded in close proximity to the small molecules that induced them.

Multi-view representation alignment can be achieved through a variety of methods, including distance-based, similarity-based, and correlation-based alignment. One classic method for representation alignment, which we leverage as a baseline in this paper, is *canonical correlation analysis (CCA)*.<sup>16</sup> CCA takes a pair of datasets  $X = [x_1 \dots x_n]$  and  $Y = [y_1 \dots y_m]$  and seeks to identify vectors  $a \in \mathcal{R}^n$  and  $b \in \mathcal{R}^m$  such that

$$(a', b') = \operatorname{argmax} \operatorname{corr}_{a,b}(a^T X, b^T Y)$$

The resultant random variables  $U = a^T X$  and  $V = b^T Y$  are the first pair of canonical variables. This process can be iteratively repeated up to  $\min(m, n)$  times with the restriction that each subsequent pair of canonical variables are uncorrelated with the previous pairs. Taken together, the procedure produces a linear mapping from the datasets  $X$  and  $Y$  that maximizes the element-wise correlation between the embeddings of paired rows from the two datasets.

A wide range of additional methods for multi-modal alignment have been proposed since CCA, including methods to align embeddings using distance-based, similarity-based, correlation-based, and ranking-based penalties during training.<sup>17</sup>

Ranking-based methods for multi-view representation alignment, such as that described by Deng et al.,<sup>18</sup> allow the incorporation of ranking information into the training procedure, which may be important in tasks such as gene expression where perturbation signals may be small relative to baseline state. In addition, the field of rank-based embedding learning is intertwined with a broader literature of uni-modal embedding learning, which pioneered such architectures as Siamese<sup>19,20</sup> and Triplet networks.<sup>21</sup> These networks optimize embeddings to bring similar data together while driving dissimilar data apart. An analysis of best practices working with this architecture can be found in Wu et al.<sup>22</sup>

### 3. Methods

#### 3.1. Dataset Preparation

##### 3.1.1. Data Acquisition and Subsetting

All raw data in this study comes from the Next-Generation Connectivity Map (CMap) provided by the LINCS Consortium and the NIH.<sup>7</sup> Analyses were conducted using the so-called "Level 3" L1000 data as described in Subramanian et al (available for download at <https://www.ncbi.nlm.nih.gov/geo/query/acc.cgi?acc=GSE70138> and <https://www.ncbi.nlm.nih.gov/geo/query/acc.cgi?acc=GSE92742>). The raw data comes in the form of gene expression profiles generated using the L1000 technology, a low-cost assay which measures 978 "landmark" genes that have been deemed representative of the full transcriptome. The CMAP contains data from a variety of chemical and genetic perturbations applied to a range of human cell lines, along with several control samples per plate treated with buffer. In order to eliminate as many sources of variance as possible beyond drug structure and cellular response, we limited our analysis to experiments conducted on the PC3 cell line and incubated with small molecules for 24 hours at a dose of  $10\mu\text{m}$ . For drug structures, we used the SMILES<sup>23</sup> structures provided by LINCS, which we canonicalized to a consistent format using RDKit.<sup>24</sup>

Data was partitioned 80-10-10 into training, validation, and test sets by experimental plate ID. A fixed random seed was chosen prior to any modeling that would maximize the number of unseen chemical structures represented in the validation and test sets. The test set was untouched until the final evaluation of models selected based on performance in the validation set. Breakdown of the splits is in Table 1 of the Appendix.

##### 3.1.2. Preprocessing and Feature Engineering

Gene expression intensity values from the training, validation, and test sets were centered and scaled at the gene-level based on the mean and standard deviation of each gene intensity across the training set. For each gene expression profile representing a chemical perturbation, we then computed four core sets of features to power our baselines and deep representations: the post-perturbational gene expression itself, corresponding gene expression intensities from a control signature on the same plate, the  $\log_2$  fold-change between the perturbation and control signatures, and the difference between these gene expression signatures.

For our initial baseline implementations of Canonical Correlation Analysis, we pre-computed features for each drug based on classical and state-of-the-art numerical representations of small molecules. For the former, we used extended-connectivity fingerprints as implemented in RDKit, a standard representation used in many computational chemistry applications.<sup>25</sup> For more modern features, we used the deep representations described in Yang et al, which achieved state-of-the-art performance in predicting 128 biophysical properties from the PubChem Bioassay database.<sup>2,26</sup>

### 3.2. *Canonical Correlation Analysis*

Canonical Correlation Analysis was performed using the CCA function implemented in SciKit Learn.<sup>27</sup> CCA models were fit in all cases using only the data in the training set, and then used to transform the gene expression and chemical structures in the test set.

Default settings from SciKit Learn’s CCA function were used, with two exceptions: first, the number of components was set to 50. The number 50 was chosen because a preliminary benchmark ranging from 5-125 components showed that 50 components had mildly superior performance in retrieval tasks on the validation set. Second, the maximum number of iterations were increased to 1000, since some initial experiments failed to converge at the default setting of 500.

### 3.3. *Deep Coordinated Representation Learning Algorithm*

We designed a cross-model ranking algorithm to learn representations of chemical structure and gene expression that would each be jointly optimized to facilitate small molecule retrieval from gene expression signatures.

An overview of this algorithm is depicted in Figure 1. In brief, gene expression profiles and drug structures are each embedded through separate neural networks into a shared embedding space. These networks are optimized together to produce representations that minimize the distance in embedding space between gene expression signatures and the drugs that induced them, while maximizing the distance between transcriptional signatures and the embeddings of other structures. Below we describe the components of this network and its training in more detail.

#### 3.3.1. *Gene Expression and Drug Embedding*

Gene expressions are embedded using self-normalizing neural networks, which are feedforward neural networks that employ the SeLU activation function.<sup>28</sup> The depth and shape of the hidden layers was left, in principle, as a hyperparameter, though in practice we generally found two hidden units of size 1024 and 512 between the input and embedding layers to give adequate performance. In addition, we employed AlphaDropout for regularization on the hidden layers, the exact value of which was left as a hyperparameter but generally set to 0.1. No activation function or dropout was used before the final embedding layer. A natural source of data augmentation was employed by randomly sampling only one control signature on each iteration of the algorithm, which meant that every epoch saw a slightly different featurization of every sample. A histogram of the number of controls per plate can be found in the Appendix.

Chemical structures were embedded using a message-passing neural network passed into a feedforward neural network. The message-passing network was initialized using the same message-passing network from Yang et al described above and used as a baseline feature set for CCA. The MPN was then allowed to be fine-tuned in tandem with the feedforward layers. The number of hidden layers was a hyperparameter usually set to one, and the embedding layer was of identical architecture to the embedding layer of the gene expression encoder.

For all of our reported experiments, gene expressions and drug structures were embedded into a 128 dimensional space.

### 3.3.2. Loss Functions and Sampling Scheme

We developed customized margin-based triplet and quadruplet losses for our task. As described in Wu et al,<sup>22</sup> an adaptive margin loss for embedding learning can be defined over two data points  $i$  and  $j$  as

$$l^{margin} := (\alpha + y_{i,j}(D_{ij} - \beta))_+$$

, where  $D$  is distance function (here euclidean distance),  $\alpha$  defines a permissible margin of separation,  $\beta$  controls the boundary between positive and negative pairs, and  $y_{i,j}$  is an indicator variable equal to 1 if  $i$  and  $j$  are of the same class and 0 otherwise.

Given this margin loss, we first explored cross-modal triplet networks<sup>18,21</sup> to align gene expression embeddings to molecular structure embeddings. In these networks, we provide the loss function with an *anchor* embedding of one modality and with one *positive* (matching) and one *negative* (non-matching) embedding of the other modality. We then define the triplet loss as the sum of the margin losses between (a) the anchor and the positive embedding, and (b) and the anchor and the negative embedding. The network is thus optimized to bring the positive embedding within the margin of the anchor and negative embedding outside the margin. To give an example: if the anchor is a drug structure, the positive example is a gene expression signature that was induced by that drug structure, and the negative example is a gene expression signature induced by some other molecular structure. The loss function then tries to force the gene expression and its corresponding small molecule structure toward each other in embedding space and away from the other drug embedding. Throughout this paper, we refer to our triplet networks as "Gene Expression-First" if their anchor embeddings are gene expressions and their positive/negative embeddings are drug structures, and as "Chemical Structure-First" otherwise.

We also explored a quadruplet design that combined the so-called "Gene expression-First" and "Chemical Structure-First" losses. In the quadruplet architecture, we sample a gene expression signature as anchor, positive and negative small molecule structures, and an additional gene expression signature induced by the negative small molecule structure. We then compute both the "Gene expression-first" triplet margin loss using the anchor gene expression signature and two molecular structures, as well as the "Chemical structure-first" margin loss using the first structure embedding as an anchor and the two gene expression embeddings as positive and negative examples. These two margin-based triplet losses are then summed together to form the quadruplet margin loss.

For sampling, we adapted the distance-weighted sampling scheme described in Wu et al, which was successful with their margin-based approach.<sup>22</sup> Since our goal is to learn to rank across modalities, we precomputed the average distance in *gene expression space* between every pair of small molecule structures in the dataset. This was performed by computing the average of the post-perturbational signatures induced by each small molecule and computing their

pairwise correlations. These pairwise correlations were then used to guide distance-weighted uniform sampling between among potential negative perturbagens.

### 3.3.3. *Training and Hyperparameter Selection*

Each model was trained on a single Nvidia GeForce GTX 1080 GPU for a maximum of 100 epochs. Early stopping was used to select the model with the best mean reciprocal rank on the validation set. Training was conducted using the Adam optimizer<sup>29</sup> with a learning rate of  $3e^{-4}$ . Hyperparameters that we manually explored included the depth of the feedforward neural networks (ranging from 0-3 hidden layers), the dropout rate (ranging 0-0.2), activation functions (sigmoid vs vs ReLU vs SeLU), and transforming gene expressions intensities to ranks. This limited manual hyperparameter search identified the values described above which we used in all experiments.

## 3.4. *Experiments*

We evaluated our coordinated representation learning strategy using an information-retrieval task. Specifically, for each perturbational gene expression profile in the test set, we rank all small molecules based on their correlation to that perturbation in the induced, aligned embedding space. We then use the standard information retrieval metrics *median rank* (MR), *mean reciprocal rank* (MRR), and *Hits or Recall @ K* to score the quality of the embeddings for retrieval purposes.<sup>30</sup> In addition, we plot the empirical cumulative distribution function of the ranks of the true perturbagen among the results. This is equivalent to a continuous-valued Hits @ K for all possible K in this dataset, and allows for a visual comparison between experiments.

Successful coordinated representation learning requires both learning rich representations of GE and chemical data, as well as the aligning them to each other. To test these separately and together, the above evaluations were repeated in the following ablation studies:

**Featurization.** Embeddings were systematically replaced with various alternative approaches to featurization. Chemical structures were replaced with Morgan Fingerprints and a state-of-the-art message passing neural network optimized for biophysical activity, which happens to be the same architecture used in the molecule embedder in our network. Gene expression embeddings were replaced in the ablation study as raw log2 fold changes to make it computational tractable.

**Loss Function for Deep Model** Results are reported for both triplet margin training strategies as well as for the training strategy without quadruplet margin loss function.

**Alignment** For all ablation studies in which non-learned features were used, CCA was applied as described above in order to align the features as best as linearly possible. In addition, we ran the evaluation on the coordinated embeddings with and without post-processing with CCA to test how complete the alignment process had been.

**Test Set** All above evaluations were run twice: First on the entire test set, to evaluate the method’s ability to generalize to unseen gene expression signatures on new plates. Second, we evaluated generalization to exclusively unseen molecules, by computing retrieval scoring specifically on the subset of the test set whose perturbagens were not present in the training

set.

### 3.5. Source Code

The source code developed for us in this project is freely available on Github at [https://github.com/sgfin/molecule\\_ge\\_coordinated\\_embeddings](https://github.com/sgfin/molecule_ge_coordinated_embeddings).

## 4. Results

Results are reported in Figure 2, Table 1, and Appendix Figure 2. We summarize here:

**Featurization** Deep coordinated embeddings of perturbational signatures and small molecules – both individually and in concert – improved retrieval performance on all metrics.

**Loss Function for Deep Model** The model trained with the quadruplet margin loss function outperformed both triplet margin training strategies.

**Alignment** Post-processing the coordinate embeddings appeared to slightly improve performance on all models, though the improvement was smaller for the quadruplet model.

**Test Set** Restricting the test set to previously unseen compounds caused a marked drop in performance of all models, though the relative performance of models was generally consistent.

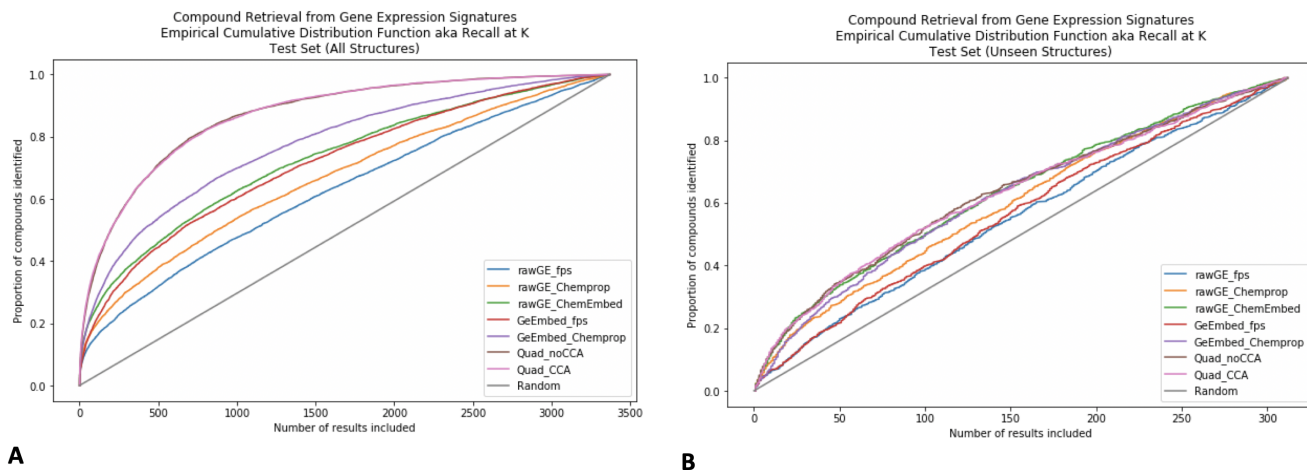


Fig. 2. Empirical CDF representing the Recall @ K for all possible K in the dataset. As can be seen in panel A, deep encodings improve recall over all other feature types. In panel B, the same general trends appear to hold, but performance is markedly worse for all methods. ECDF for Triplet-based models is found in the Appendix.

## 5. Discussion

### 5.1. Observations

In this paper, we have sought to present both a new biomedical machine learning task – cross-modal retrieval of molecular structure from perturbational signatures – as well as a set of approaches to benchmark future work on this task.

Table 1. Information retrieval drug retrieval tasks. MR=median rank, MRR=mean reciprocal rank, H@K=Hits (Recall) at K.

Input		Test Set, All (3370 total)					Test Set, Unseen Mols (312 total)				
GE Encoding	Chemical Encoding	Alignment	MR	MRR	H@10	H@100	H@500	MR	MRR	H@10	H@100
Raw	Morgan FP	CCA	1102	0.037	0.063	0.154	0.319	134	0.039	0.065	0.389
Raw	Chemprop	CCA	874	0.045	0.078	0.192	0.380	116.5	0.055	0.096	0.447
Raw	Quadruplet	CCA	604	0.057	0.099	0.242	0.460	100	0.059	0.123	0.503
Quadruplet	Morgan FP	CCA	644	0.035	0.063	0.206	0.444	131	0.041	0.068	0.400
Quadruplet	Chemprop	CCA	403	0.049	0.091	0.267	0.538	101	0.048	0.079	0.499
Triplet-GE-First	Triplet-GE-First	CCA	236	0.070	0.123	0.341	0.666	97.5	<b>0.062</b>	0.126	0.511
Triplet-Chem-First	Triplet-Chem-First	CCA	240	0.069	0.122	0.346	0.673	103	0.055	0.095	0.487
Quadruplet	Quadruplet	CCA	<b>196</b>	<b>0.073</b>	<b>0.135</b>	<b>0.384</b>	0.706	<b>93</b>	0.056	<b>0.136</b>	0.521
Triplet-GE-First	Triplet-GE-First	None	306	0.055	0.099	0.289	0.626	101	0.051	0.098	0.499
Triplet-Chem-First	Triplet-Chem-First	None	260	0.058	0.102	0.322	0.663	106.5	0.049	0.104	0.488
Quadruplet	Quadruplet	None	199	0.066	0.122	0.372	<b>0.711</b>	96.5	0.060	0.124	<b>0.523</b>

Our results indicate that the task appears feasible, and that the richer models afforded by recent advances in deep learning show marked improvements over baseline methods.

Nevertheless, generalization to unseen molecular libraries – arguably the greatest promise of this method over pure connectivity mapping approaches – seems to be very challenging. It is interesting to note, however, that while performance on the unseen molecule set was poor, the most expressive models still had the highest performance; this seems to indicate that increased model capacity rather than merely better regularization will be necessary to generalize to these molecules.

We are intrigued by the observation that our quadruplet loss appeared to perform better than either triplet loss in terms of retrieval performance on the test sets. In addition, we note that while CCA seemed to improve the alignment of embeddings in every model, the embeddings trained with the quadruplet loss changed very little with CCA, to the point that the eCDF curves almost perfectly overlay each other.

## 5.2. *Limitations and Future Work*

From the perspective of task formulation, one area of future interest is the development of custom metrics to score model ranks. As it stands, the evaluation strategy counts the exact perturbation as correct, and all other small molecules as equally incorrect. This will potentially under-estimate model performance, as it ignores the possibility of other plausible candidates. It would therefore be useful to consider metrics that incorporate functional or structural similarity to provide non-zero scores to reasonable alternatives. An additional concern is that the evaluation on unseen molecular structures is limited to only 300 molecules, which means that those scores will likely have higher bias and variance. Finally, expanding the task to include – and ideally translate between – perturbational signatures from multiple cell types and dosages will be essential to assessing and optimizing generalizability to new biological settings.

From the perspective of model formulation, there are several follow-up experiments that we are excited to pursue that would require only additional computational and human resources. These include a more dedicated hyperparameter optimization search and the implementation of test-time augmentation by ensembling predictions over repeat control sampling. In addition, we would like to compute confidence intervals for all experimental values computed by bootstrapping. Such exercises will be indispensable in identifying which if any of the comparisons in performance may be due to statistical aberration rather than substantive difference.

Slightly more sophisticated follow-up work includes the investigation of more intelligent pretraining strategies and negative sampling techniques, which may prove essential for improved generalization. In addition, as described in Li et al, there are a wide variety of additional architectures that could be tried for this task, such as Cross-Modal Factor Analysis, Kernel CCA, and a range of novel deep learning architectures.<sup>17</sup> Anecdotally, one model which we did begin to explore was Deep Canonical Correlation Analysis,<sup>31</sup> which on first implementation has not produced useful embeddings for this task. These results were not included formally in this work, however, due to insufficient time to ensure the results weren't due to poor hyperparameters.

Of greatest interest to us as authors is a deep examination of the failure modes that take place when the model tries to generalize to unseen molecules. In particular, we would like to characterize what precisely are the properties of chemical libraries that do or do not enable mutual generalizability. It is our hope that elucidating these pitfalls could lead both to better algorithms and to better chemical libraries.

## 6. Conclusion

We present a method for jointly modeling chemical structure and corresponding transcriptional perturbations, using deep coordinated representation learning. The method shows promise on a benchmark task of unseen gene expression signatures, but fails to adequately generalize to entirely unseen chemical structures. Future directions to overcome this generalization gap could yield interesting fruit for both chemical biology and library design.

## 7. Acknowledgements

The authors thank Connor Coley and Kyle Swanson for graciously providing the pretrained chemical embedder from Yang et al.<sup>2</sup> S.G.F. was supported by training grant T32GM007753 from the National Institute of General Medical Science. M.B.A.M. is funded in part by National Institutes of Health: National Institutes of Mental Health grant P50-MH106933 as well as a Mitacs Globalink Research Award. The content is solely the responsibility of the authors.

## References

1. T. Hansson, C. Oostenbrink and W. van Gunsteren, Molecular dynamics simulations, *Current opinion in structural biology* **12**, 190 (2002).
2. K. Yang, K. Swanson, W. Jin, C. W. Coley, P. Eiden, H. Gao, A. Guzman-Perez, T. Hopper, B. Kelley, M. Mathea *et al.*, Analyzing learned molecular representations for property prediction, *Journal of chemical information and modeling* (2019).
3. Y.-C. Lo, S. E. Rensi, W. Torng and R. B. Altman, Machine learning in chemoinformatics and drug discovery, *Drug discovery today* **23**, 1538 (2018).
4. M. Krallinger, O. Rabal, A. Lourenco, J. Oyarzabal and A. Valencia, Information retrieval and text mining technologies for chemistry, *Chemical reviews* **117**, 7673 (2017).
5. A. Musa, L. S. Ghorraie, S.-D. Zhang, G. Glazko, O. Yli-Harja, M. Dehmer, B. Haibe-Kains and F. Emmert-Streib, A review of connectivity map and computational approaches in pharmacogenomics, *Briefings in bioinformatics* **19**, 506 (2017).
6. J. Lamb, E. D. Crawford, D. Peck, J. W. Modell, I. C. Blat, M. J. Wrobel, J. Lerner, J.-P. Brunet, A. Subramanian, K. N. Ross *et al.*, The connectivity map: using gene-expression signatures to connect small molecules, genes, and disease, *science* **313**, 1929 (2006).
7. A. Subramanian, R. Narayan, S. M. Corsello, D. D. Peck, T. E. Natoli, X. Lu, J. Gould, J. F. Davis, A. A. Tubelli, J. K. Asiedu *et al.*, A next generation connectivity map: L1000 platform and the first 1,000,000 profiles, *Cell* **171**, 1437 (2017).
8. A. Musa, S. Tripathi, M. Kandhavelu, M. Dehmer and F. Emmert-Streib, Harnessing the biological complexity of big data from lincs gene expression signatures, *PloS one* **13**, p. e0201937 (2018).
9. T.-P. Liu, Y.-Y. Hsieh, C.-J. Chou and P.-M. Yang, Systematic polypharmacology and drug repurposing via an integrated l1000-based connectivity map database mining, *Royal Society open science* **5**, p. 181321 (2018).

10. N. R. Clark, K. S. Hu, A. S. Feldmann, Y. Kou, E. Y. Chen, Q. Duan and A. Maayan, The characteristic direction: a geometrical approach to identify differentially expressed genes, *BMC bioinformatics* **15**, p. 79 (2014).
11. Y. Donner, S. Kazmierczak and K. Fortney, Drug repurposing using deep embeddings of gene expression profiles, *Molecular pharmaceutics* **15**, 4314 (2018).
12. A. B. Dincer, S. Celik, N. Hiranuma and S.-I. Lee, Deepprofile: Deep learning of cancer molecular profiles for precision medicine, *bioRxiv*, p. 278739 (2018).
13. L. Rampásek, D. Hidru, P. Smirnov, B. Haibe-Kains and A. Goldenberg, Dr. vae: improving drug response prediction via modeling of drug perturbation effects, *Bioinformatics* (2019).
14. J. Cheng, Q. Xie, V. Kumar, M. Hurle, J. M. Freudenberg, L. Yang and P. Agarwal, Evaluation of analytical methods for connectivity map data, in *Biocomputing 2013*, (World Scientific, 2013) pp. 5–16.
15. R. Hodos, P. Zhang, H.-C. Lee, Q. Duan, Z. Wang, N. R. Clark, A. Maayan, F. Wang, B. Kidd, J. Hu *et al.*, Cell-specific prediction and application of drug-induced gene expression profiles, in *Pacific Symposium on Biocomputing*, 2017.
16. H. Hotelling, Relations between two sets of variates, in *Breakthroughs in statistics*, (Springer, 1992) pp. 162–190.
17. Y. Li, M. Yang and Z. M. Zhang, A survey of multi-view representation learning, *IEEE Transactions on Knowledge and Data Engineering* (2018).
18. C. Deng, Z. Chen, X. Liu, X. Gao and D. Tao, Triplet-based deep hashing network for cross-modal retrieval, *IEEE Transactions on Image Processing* **27**, 3893 (2018).
19. G. Koch, R. Zemel and R. Salakhutdinov, Siamese neural networks for one-shot image recognition, in *ICML deep learning workshop*, 2015.
20. T. M. Filzen, P. S. Kutchukian, J. D. Hermes, J. Li and M. Tudor, Representing high throughput expression profiles via perturbation barcodes reveals compound targets, *PLoS computational biology* **13**, p. e1005335 (2017).
21. E. Hoffer and N. Ailon, Deep metric learning using triplet network, in *International Workshop on Similarity-Based Pattern Recognition*, 2015.
22. C.-Y. Wu, R. Manmatha, A. J. Smola and P. Krahenbuhl, Sampling matters in deep embedding learning, in *Proceedings of the IEEE International Conference on Computer Vision*, 2017.
23. D. Weininger, A. Weininger and J. L. Weininger, Smiles. 2. algorithm for generation of unique smiles notation, *Journal of chemical information and computer sciences* **29**, 97 (1989).
24. G. Landrum *et al.*, Rdkit: Open-source cheminformatics (2006).
25. D. Rogers and M. Hahn, Extended-connectivity fingerprints, *Journal of chemical information and modeling* **50**, 742 (2010).
26. Y. Wang, J. Xiao, T. O. Suzek, J. Zhang, J. Wang, Z. Zhou, L. Han, K. Karapetyan, S. Dracheva, B. A. Shoemaker *et al.*, Pubchem’s bioassay database, *Nucleic acids research* **40**, D400 (2011).
27. F. Pedregosa, G. Varoquaux, A. Gramfort, V. Michel, B. Thirion, O. Grisel, M. Blondel, P. Prettenhofer, R. Weiss, V. Dubourg *et al.*, Scikit-learn: Machine learning in python, *Journal of machine learning research* **12**, 2825 (2011).
28. G. Klambauer, T. Unterthiner, A. Mayr and S. Hochreiter, Self-normalizing neural networks, in *Advances in neural information processing systems*, 2017.
29. D. P. Kingma and J. Ba, Adam: A method for stochastic optimization, *arXiv preprint arXiv:1412.6980* (2014).
30. C. Manning, P. Raghavan and H. Schütze, Introduction to information retrieval, *Natural Language Engineering* **16**, 100 (2010).
31. G. Andrew, R. Arora, J. Bilmes and K. Livescu, Deep canonical correlation analysis, in *International conference on machine learning*, 2013.

## Appendix

Table 2. Details of train-validation-test splits.

Split	# Gene Expression Signatures	# Distinct Molecules	# Molecules not in Train
Train	29,548	6318	N/A
Validation	2642	2248	307
Test	3370	3370	312

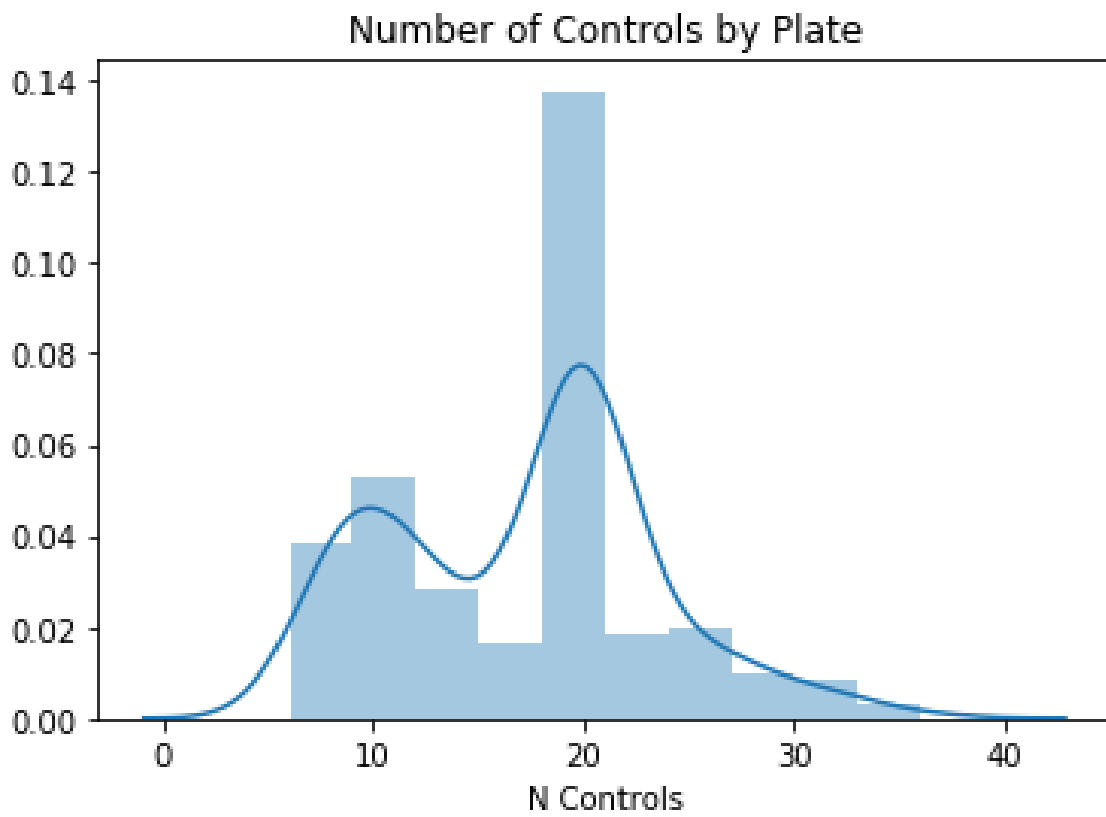


Fig. 3. Histogram showing the number of controls per plate.

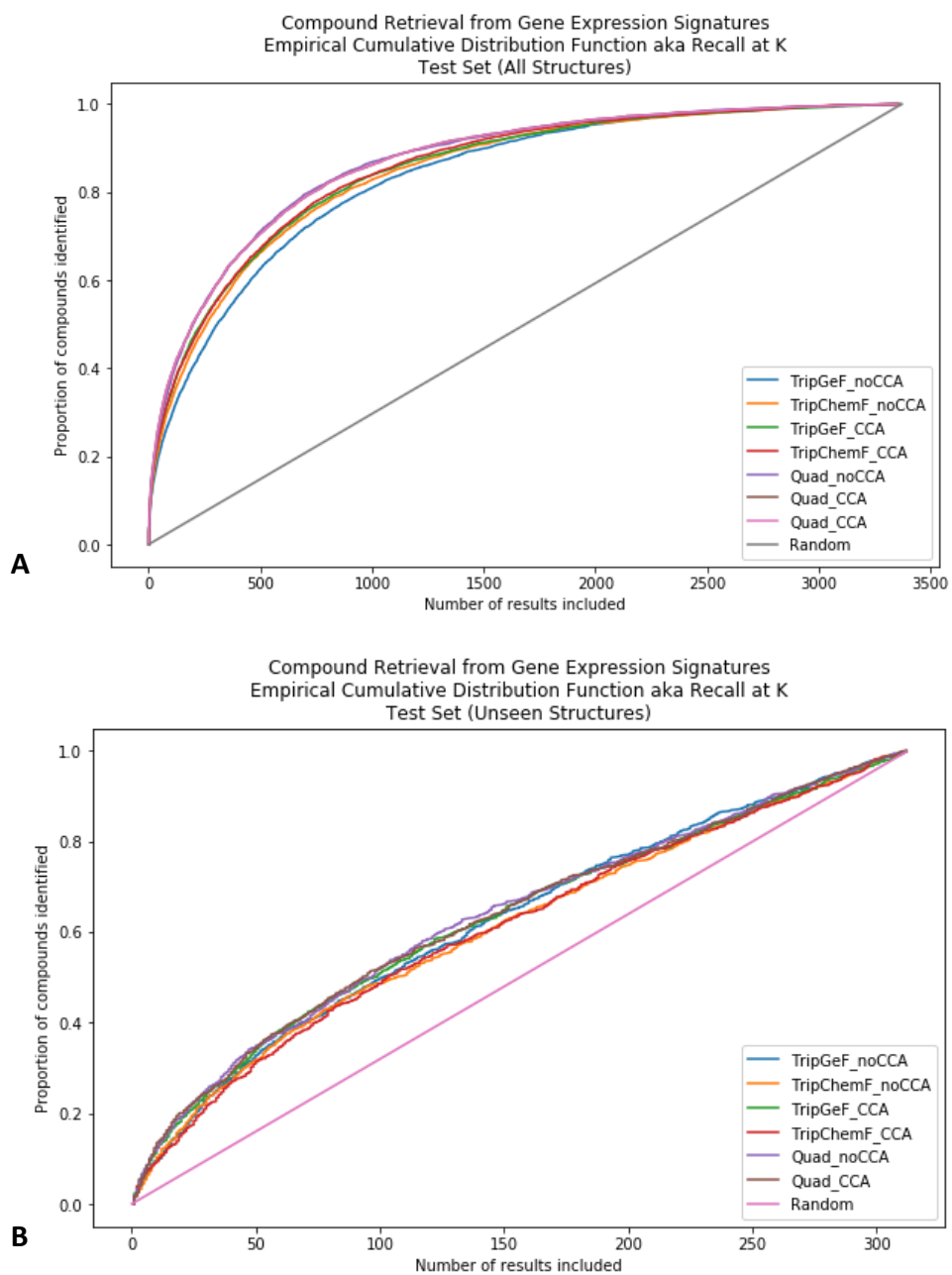


Fig. 4. Empirical CDF comparing triplet-based models to the quadruplet-based model. Represents the Recall @ K for all possible K in the dataset.